Journal of MECHANICAL ENGINEERING
– Strojnícky časopis

VOLUME 65, NO 1, 2015

Print ISSN 0039-2472
On-line ISSN 2450-5471

pp. 77 – 92
DOI:10.1515/scjme-2016-0005

ANALYSIS OF PIEZOELECTRIC SEMICONDUCTING SOLIDS BY MESHLESS METHOD

STAŇÁK, P.[1], SLÁDEK, J.[1], SLÁDEK, V.[1]

[1] *Institute of Construction and Architecture, Slovak Academy of Sciences, Dúbravská cesta 9, 845 03 Bratislava, Slovak Republic, email: peter.stanak@savba.sk*

Abstract: In this paper, a meshless local Petrov-Galerkin (MLPG) method is proposed to calculate mechanical and electrical responses of three-dimensional piezoelectric semiconductors under static load. The analyzed solid is discretized by a set of generally distributed nodal points distributed over 3D geometry. Local integral equations (LIEs) are derived from the weak form of governing equations over small local subdomains. The subdomains have a spherical shape with a nodal point located in its centre. A unit step function is used as the test functions in the local weak-form. The moving least-squares (MLS) method is adopted for the approximation of the physical quantities in the LIEs. The proposed MLPG method is verified by using the corresponding results obtained with the finite element method. Numerical examples are presented and discussed for various boundary conditions and loading scenarios to show the performance of the developed MLPG method for analysis piezoelectric semiconducting solids.

KEYWORDS: piezoelectric semiconductors, meshless local Petrov-Galerkin (MLPG) method, MLS approximation scheme

1. Introduction

Smart materials and especially piezoelectric materials have received great attention in recent years [4]. These materials are extensively utilized as transducers, sensors and actuators in many engineering fields. Piezoelectric materials have anisotropic properties. Except this complication, electric and mechanical fields are coupled each other and the governing equations are much more complex than those in the classical elasticity. The approach usually adopted in treating piezoelectric media is to simplify Maxwell's equations by neglecting magnetic effects, conduction, displacement currents and free charges. This classical, electrically quasistatic theory of piezoelectric bodies, which is sufficient for nearly all engineering applications, is clearly formulated for plate problems in a book by Tiersten [2].

In most cases, piezoelectric crystals and ceramics are treated as nonconducting dielectrics but in reality there is no sharp division separating conductors from dielectrics. Real materials more or less have some conduction [3]. Thus special interest should be devoted to piezoelectric composed materials exhibiting semiconducting properties. In such a case, the electric field produces currents and space charge resulting in dispersion of elastic waves. The interaction between a traveling acoustic wave and mobile charges in piezoelectric semiconductors is called an acoustoelectric effect.

The acoustoelectric effect and amplification of acoustic waves can be achieved through composite structures of piezoelectric dielectrics and nonpiezoeletric semiconductors, which have led to the development of acoustoelectric devices. Usually, these kind devices are made of layered structure where a thin or thick layer is deposited on elastic or piezoelectric substrate [4]. Piezoelectric semiconductors have been used to make devices for acoustic wave

amplification [5, 6] and acoustic charge transport [7] based on the acoustoelectric effect. Fracture analysis of piezoelectric semiconductors was recently performed by Sladek et al. [8].

Numerical analysis of piezoelectric devices has been dominated by the mesh-based methods such as finite element method (FEM) and boundary element method (BEM). FEM is widely used in design of structures [9] incorporating piezoelectric materials, however it possesses some drawbacks, e.g. shear-locking of elements during modeling of thin-walled structures that is eliminated only at high computational cost and lower accuracy. BEM has been applied to analysis of piezoelectric materials [10, 11], however it is limited by the unavailability of fundamental solutions for 3-D problems in piezoelectric anisotropic materials.

Meshless methods for solution of various boundary value problems are powerful alternative to mesh-based techniques. Meshless methods are also characterized by high adaptivity and low cost to prepare input and output data for numerical analyses. Many drawbacks of mesh-based methods can be efficiently eliminated if only nodal points are used instead of finite elements. The meshless local Petrov-Galerkin (MLPG) method is considered as a fundamental base for the derivation of many meshless formulations, since trial and test functions can be chosen from different functional spaces. The MLPG method introduced by Atluri [12] and Sladek et al. [13], using a Heaviside step function as the test functions, has been applied to solve 2-D homogeneous piezoelectric dielectric problems in paper by Sladek et al. [14]. Recently, meshless method (MLPG) was applied to analyze continuously nonhomogeneous piezoelectric solids under a mechanical or electrical load [15].

The MLPG has been successfully applied to various problems related to piezoelectricity including thermopiezoelectricity [16], piezoelectric rectangular and laminated plates [17, 18].

As a special case of 3-D problems axisymmetric solids and axisymmetric circular plates [19, 20]. Axial symmetry of assumed geometry reduces the original 3-D problem into a 2-D problem in the angular cross section. Present paper thus gives an extension of the MLPG method to 3-D piezoelectric semiconducting solids, since previous works only included 3-D elastic and piezoelectric dielectric solids [21, 22]. The coupled electro-mechanical fields for piezoelectric semiconducting material are described by constitutive relations and governing partial differential equations (PDEs). Nodal points are spread on the analyzed domain without any limitations on their mutual position. Small local subdomain of spherical shape is introduced around each nodal point. Local integral equations (LIEs) constructed from governing PDEs are defined over these spherical subdomains. Heaviside unit step function is applied as a test function in each local subdomain [23]. Numerical integrations can be easily carried out over the local subdomains if a simple shape like a sphere is chosen for their geometry. Moving Least-Squares (MLS) approximation scheme [12, 24] is used to approximate the spatial variations of all physical fields in terms of specific nodal values. The essential boundary conditions on the global boundary are specified by the collocation of the MLS approximations for prescribed field quantities at the boundary nodes. Numerical examples are presented for the piezoelectric semiconductor of cylindrical shape to assess the applicability of the proposed MLPG method.

2. Basic equations for piezoelectric semiconductors

Governing equations describing the stationary behavior of 3D piezoelectric semiconducting body Ω under static loading are given by the force equilibrium equation, the first scalar Maxwell's equation and the equation of conservation of charge of electrons [5] as

$$\sigma_{ij,j}(\mathbf{x}) + X_i(\mathbf{x}) = 0 \tag{1}$$

$$D_{i,i}(\mathbf{x}) = qM(\mathbf{x}) \tag{2}$$

$$J_{i,i}(\mathbf{x}) = 0 \tag{3}$$

where $\sigma_{ij}(\mathbf{x})$ is the stress tensor, $D_i(\mathbf{x})$ is the vector of electric displacements, $J_i(\mathbf{x})$ is the vector of electric current, $X_i(\mathbf{x})$ is vector of body forces, q is the electric charge of the electron (assuming n-type semiconductivity) and $M(\mathbf{x})$ is the change of the electron density producing a net space charge (density of free electric charge). Cartesian coordinates are specified for 3D case as $\mathbf{x} = (x_1, x_2, x_3)$. Recall that in stationary problems, the Maxwell equations are reduced to the Gauss law, provided that the magnetic field is not present and the intensity of electric field is expressed as the gradient of a scalar potential.

Constitutive equations of the piezoelectric material represent the coupling of the mechanical and electrical fields. The piezoelectric constitutive equations given by White [5] are representing the coupling of the mechanical and electrical fields and also electrical current. In the case of stationary problems, the constitutive relationships become

$$\sigma_{ij}(\mathbf{x}) = c_{ijkl}(\mathbf{x})\varepsilon_{kl}(\mathbf{x}) - e_{kij}(\mathbf{x})E_k(\mathbf{x}) \tag{4}$$

$$D_j(\mathbf{x}) = e_{jkl}(\mathbf{x})\varepsilon_{kl}(\mathbf{x}) + h_{jk}(\mathbf{x})E_k(\mathbf{x}) \tag{5}$$

$$J_i(\mathbf{x}) = qM_0(\mathbf{x})\mu_{ij}(\mathbf{x})E_j(\mathbf{x}) - qd_{ij}(\mathbf{x})M_{,j}(\mathbf{x}) \tag{6}$$

where $c_{ijkl}(\mathbf{x})$, $e_{ijk}(\mathbf{x})$, $h_{ij}(\mathbf{x})$, $\mu_{ij}(\mathbf{x})$ and $d_{ij}(\mathbf{x})$ are the elastic, piezoelectric, dielectric, electron mobility and carrier diffusion material coefficients, respectively. Recall that $M_0(\mathbf{x})$ is the density of electrons in unloaded state and producing no net space charge in contrast to $M(\mathbf{x})$.

The strain tensor ε_{ij} and the electric field vector E_j are related to the displacements u_i and the electric potential ψ by

$$\varepsilon_{ij} = \frac{1}{2}\left(u_{i,j} + u_{j,i}\right), \tag{7}$$

$$E_j = -\psi_{,j}\ . \tag{8}$$

For the mechanical field following essential and natural boundary conditions are assumed:

$$u_i(\mathbf{x}) = u_i(\mathbf{x}), \qquad \text{on} \quad \Gamma_u,$$
$$t_i(\mathbf{x}) = \sigma_{ij}n_j = t_i(\mathbf{x}), \qquad \text{on} \quad \Gamma_t,$$

for the electrical field:

$$\psi(\mathbf{x}) = \psi(\mathbf{x}), \qquad \text{on} \quad \Gamma_p,$$
$$n_i D_i(\mathbf{x}) = qM(\mathbf{x}), \qquad \text{on} \quad \Gamma_q,$$

and finally for the electrical current field:

$$M(\mathbf{x}) = M(\mathbf{x}), \qquad \text{on} \quad \Gamma_a,$$

$J_i(\mathbf{x})n_i(\mathbf{x}) = S(\mathbf{x})$, on Γ_b, note that $\Gamma = \Gamma_a \cup \Gamma_b$,

where n_j is the unit vector normal to the boundary and Γ_u is the part of the global boundary Γ with prescribed displacements, while on Γ_t, Γ_p, Γ_q, Γ_a, and Γ_b the traction vector, electric potential, surface density of the free charge, electron density, and the electric current flux are, respectively, applied.

The constitutive equations for piezoelectric semiconductors (4-6), representing the coupling of mechanical and electrical voltage and current fields, may be written for transversally isotropic 3-D piezoelectric semiconducting body poled in x_3 direction in a compact matrix form as

$$\begin{bmatrix}\sigma_{11}\\ \sigma_{22}\\ \sigma_{33}\\ \sigma_{23}\\ \sigma_{13}\\ \sigma_{12}\end{bmatrix} = \begin{bmatrix} c_{11} & c_{12} & c_{13} & 0 & 0 & 0\\ c_{12} & c_{11} & c_{13} & 0 & 0 & 0\\ c_{13} & c_{13} & c_{33} & 0 & 0 & 0\\ 0 & 0 & 0 & c_{44} & 0 & 0\\ 0 & 0 & 0 & 0 & c_{55} & 0\\ 0 & 0 & 0 & 0 & 0 & c_{66}\end{bmatrix}\begin{bmatrix}\varepsilon_{11}\\ \varepsilon_{22}\\ \varepsilon_{33}\\ 2\varepsilon_{23}\\ 2\varepsilon_{13}\\ 2\varepsilon_{12}\end{bmatrix} - \begin{bmatrix} 0 & 0 & e_{31}\\ 0 & 0 & e_{31}\\ 0 & 0 & e_{33}\\ 0 & e_{15} & 0\\ e_{15} & 0 & 0\\ 0 & 0 & 0\end{bmatrix}\begin{bmatrix}E_1\\ E_2\\ E_3\end{bmatrix}, \tag{9}$$

$$\begin{bmatrix}D_1\\ D_2\\ D_3\end{bmatrix} = \begin{bmatrix} 0 & 0 & 0 & 0 & e_{15} & 0\\ 0 & 0 & 0 & e_{15} & 0 & 0\\ e_{31} & e_{31} & e_{33} & 0 & 0 & 0\end{bmatrix}\begin{bmatrix}\varepsilon_{11}\\ \varepsilon_{22}\\ \varepsilon_{33}\\ 2\varepsilon_{23}\\ 2\varepsilon_{13}\\ 2\varepsilon_{12}\end{bmatrix} + \begin{bmatrix} h_{11} & 0 & 0\\ 0 & h_{11} & 0\\ 0 & 0 & h_{33}\end{bmatrix}\begin{bmatrix}E_1\\ E_2\\ E_3\end{bmatrix}, \tag{10}$$

$$\begin{bmatrix}J_1\\ J_2\\ J_3\end{bmatrix} = qM_0\begin{bmatrix}\mu_{11} & 0 & 0\\ 0 & \mu_{22} & 0\\ 0 & 0 & \mu_{33}\end{bmatrix}\begin{bmatrix}E_1\\ E_2\\ E_3\end{bmatrix} - q\begin{bmatrix} d_{11} & 0 & 0\\ 0 & d_{22} & 0\\ 0 & 0 & d_{33}\end{bmatrix}\begin{bmatrix}M_{,1}\\ M_{,2}\\ M_{,3}\end{bmatrix}, \tag{11}$$

where $c_{66} = \frac{1}{2}(c_{11} - c_{12})$.

3. Formulation by the MLPG method

The MLPG method is based on the local weak form of the governing equations (1-3) that is written over local subdomain Ω_s. Local subdomain is shown in Fig. 1. Local subdomain is a small region taken for each node inside the global domain [12]. The local subdomains could be of any geometrical shape; in this paper spherical shape is used just for simplicity.

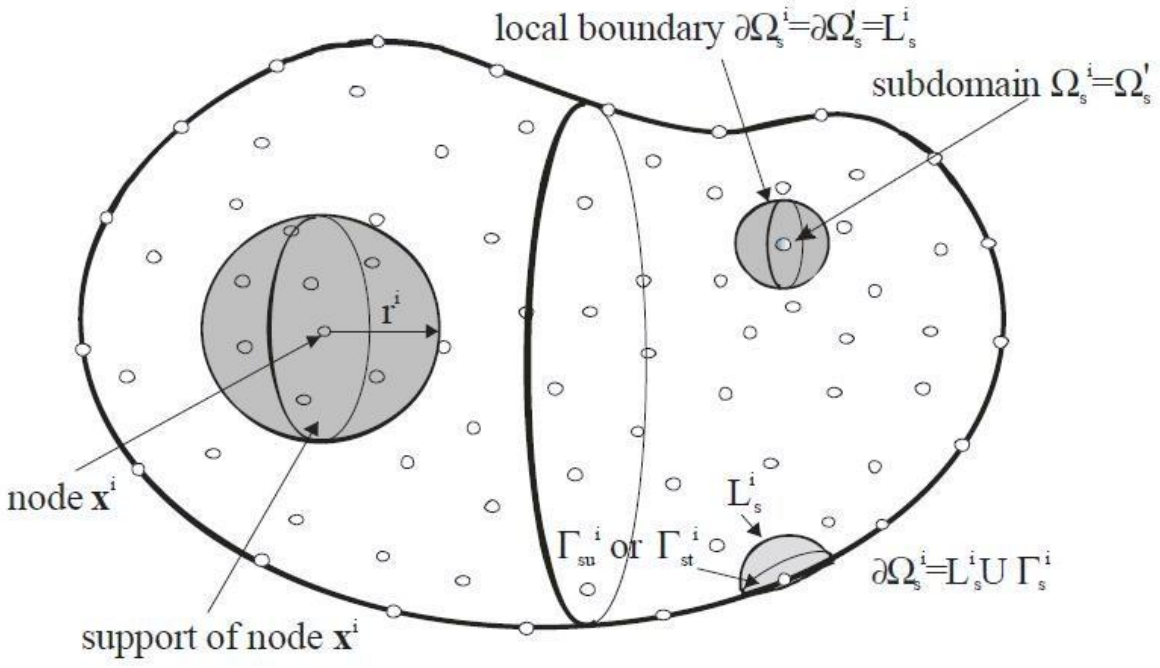

Fig. 1. Local boundaries and sub-domain for weak formulation and support domain for MLS approximation.

The local weak-form of the governing equations (1-3) can be written as

$$\int_{\Omega_s} \left\lfloor \sigma_{ij,j}(\mathbf{x}) - X_i(\mathbf{x}) \right\rfloor w_{ik}^*(\mathbf{x})\, d\Omega = 0 \tag{12}$$

$$\int_{\Omega_s} \left\lfloor D_{i,i}(\mathbf{x}) - qM(\mathbf{x}) \right\rfloor w^*(\mathbf{x})\, d\Omega = 0 \tag{13}$$

$$\int_{\Omega_s} \left\lfloor J_{i,i}(\mathbf{x}) \right\rfloor w^*(\mathbf{x})\, d\Omega = 0 \tag{14}$$

where $w_{ik}^*(\mathbf{x})$ and $w^*(\mathbf{x})$ are test functions.

Heaviside step function is chosen as the test function $w_{ik}^*(\mathbf{x})$ and $w^*(\mathbf{x})$ in each subdomain as

$$w_{ik}^*(\mathbf{x}) = \begin{cases} \delta_{ik} & \text{at } \mathbf{x} \in \Omega_s \\ 0 & \text{at } \mathbf{x} \notin \Omega_s \end{cases}, \quad w^*(\mathbf{x}) = \begin{cases} 1 & \text{at } \mathbf{x} \in \Omega_s \\ 0 & \text{at } \mathbf{x} \notin \Omega_s \end{cases}. \tag{15}$$

Local integral equations (LIEs) are formed from the local weak forms (12-14) with the use of Gauss divergence theorem and properties of selected test functions (15). Assuming the body forces $X_i(\mathbf{x})$ to be vanishing in the present case, LIEs take the following form

$$\int_{\partial\Omega_S} \sigma_{ij}(\mathbf{x}) n_j(\mathbf{x})\, d\Gamma = 0 \tag{16}$$

$$\int_{\partial\Omega_S} D_i(\mathbf{x}) n_i(\mathbf{x}) d\Gamma - \int_{\Omega_S} qM(\mathbf{x}) d\Omega = 0 \tag{17}$$

$$\int_{\partial\Omega_S} J_i(\mathbf{x}) n_i(\mathbf{x}) d\Gamma = 0 \tag{18}$$

where $n_j(\mathbf{x})$ is the unit outward normal vector to the boundary $\partial\Omega_S$ of local subdomain.

There is no requirement in the MLPG method on the test and the trial functions to be necessarily from the same functional spaces. For internal nodes, the test function is chosen as the Heaviside step function with its support on the local subdomain. The trial functions, on the other hand, are chosen in this paper to be the moving least-squares (MLS) approximation [12] over a number of nodes spread within the domain of influence. The MLS approximation is used for the approximation of displacements, electric potential field and the change of electron density in terms of scattered nodal points as

$$u_j(\mathbf{x}) = \sum_{i=1}^{n} \phi^i(\mathbf{x}) \hat{u}_j^i \quad , \psi(\mathbf{x}) = \sum_{i=1}^{n} \phi^i(\mathbf{x}) \hat{\psi}^i \quad , \quad M(\mathbf{x}) = \sum_{i=1}^{n} \phi^i(\mathbf{x}) \hat{M}^i \tag{19}$$

where the nodal values $\hat{u}_j^i$, $\hat{\psi}^i$ and $\hat{M}^i$ are so called fictitious parameters for the mechanical displacements ,electric potential and the change of electron density, respectively. The MLS shape function $\phi^i(\mathbf{x})$ is defined over a set of n nodes located in the support domain Ω_x [12]. C^1-continuity of the MLS approximation is ensured by the fourth-order spline type weight function used for the construction of the shape function given as

$$v^a(\mathbf{x}) = \begin{cases} 1 - 6\left(\dfrac{d^a}{r^a}\right)^2 + 8\left(\dfrac{d^a}{r^a}\right)^3 - 3\left(\dfrac{d^a}{r^a}\right)^4 & 0 \le d^a \le r^a \\ 0 & d^a \ge r^a \end{cases} \tag{20}$$

where $d^a = \left\| \mathbf{x} - \mathbf{x}^a \right\|$ and r^a is the radius of the circular support domain. The value of n in Eq. (19) is determined by the number of nodes lying in the support domain with radius r^a. The partial derivatives of field quantities are approximated with the use of the shape function derivatives $\phi_{,k}^i(\mathbf{x})$ and original fictitious parameters as

$$u_{j,k}(\mathbf{x}) = \sum_{i=1}^{n} \phi_{,k}^i(\mathbf{x}) \hat{u}_j^i \quad , \psi_{,k}(\mathbf{x}) = \sum_{i=1}^{n} \phi_{,k}^i(\mathbf{x}) \hat{\psi}^i \quad , M_{,k}(\mathbf{x}) = \sum_{i=1}^{n} \phi_{,k}^i(\mathbf{x}) \hat{M}^i \tag{21}$$

Applying Eqs. (19), (21) to approximation of trial functions $u_j(\mathbf{x})$, $\psi(\mathbf{x})$, $M(\mathbf{x})$ and their derivatives in constitutive relations (4-6) and their subsequent insertion into local integral equations (16-18) is leading to discretized local integral equations in the following form

$$\sum_{i=1}^{n}\hat{u}_1^i\left(\int_{\partial\Omega_S}\left[n_1c_{11}\phi_{,1}^i(\mathbf{x})+n_2c_{66}\phi_{,2}^i(\mathbf{x})+n_3c_{55}\phi_{,3}^i(\mathbf{x})\right]d\Gamma\right)+\sum_{i=1}^{n}\hat{u}_2^i\left(\int_{\partial\Omega_S}\left[n_1c_{12}\phi_{,2}^i(\mathbf{x})+n_2c_{66}\phi_{,1}^i(\mathbf{x})\right]d\Gamma\right)$$
$$+\sum_{i=1}^{n}\hat{u}_3^i\left(\int_{\partial\Omega_S}\left[n_1c_{13}\phi_{,3}^i(\mathbf{x})+n_3c_{55}\phi_{,1}^i(\mathbf{x})\right]d\Gamma\right)+\sum_{i=1}^{n}\hat{\psi}^i\left(\int_{\partial\Omega_S}\left[n_1e_{31}\phi_{,3}^i(\mathbf{x})+n_3e_{15}\phi_{,1}^i(\mathbf{x})\right]d\Gamma\right)=0 \tag{22}$$

$$\sum_{i=1}^{n}\hat{u}_1^i\left(\int_{\partial\Omega_S}\left[n_1c_{66}\phi_{,2}^i(\mathbf{x})+n_2c_{12}\phi_{,1}^i(\mathbf{x})\right]d\Gamma\right)+\sum_{i=1}^{n}\hat{u}_2^i\left(\int_{\partial\Omega_S}\left[n_1c_{66}\phi_{,1}^i(\mathbf{x})+n_2c_{11}\phi_{,2}^i(\mathbf{x})+n_3c_{44}\phi_{,3}^i(\mathbf{x})\right]d\Gamma\right)$$
$$+\sum_{i=1}^{n}\hat{u}_3^i\left(\int_{\partial\Omega_S}\left[n_2c_{13}\phi_{,3}^i(\mathbf{x})+n_3c_{44}\phi_{,2}^i(\mathbf{x})\right]d\Gamma\right)+\sum_{i=1}^{n}\hat{\psi}^i\left(\int_{\partial\Omega_S}\left[n_2e_{31}\phi_{,3}^i(\mathbf{x})+n_3e_{15}\phi_{,2}^i(\mathbf{x})\right]d\Gamma\right)=0 \tag{23}$$

$$\sum_{i=1}^{n}\hat{u}_1^i\left(\int_{\partial\Omega_S}\left[n_1c_{55}\phi_{,3}^i(\mathbf{x})+n_3c_{13}\phi_{,1}^i(\mathbf{x})\right]d\Gamma\right)+\sum_{i=1}^{n}\hat{u}_3^i\left(\int_{\partial\Omega_S}\left[n_1c_{55}\phi_{,1}^i(\mathbf{x})+n_2c_{44}\phi_{,2}^i(\mathbf{x})+n_3c_{33}\phi_{,3}^i(\mathbf{x})\right]d\Gamma\right)$$
$$+\sum_{i=1}^{n}\hat{u}_2^i\left(\int_{\partial\Omega_S}\left[n_2c_{44}\phi_{,3}^i(\mathbf{x})+n_3c_{13}\phi_{,2}^i(\mathbf{x})\right]d\Gamma\right)+\sum_{i=1}^{n}\hat{\psi}^i\left(\int_{\partial\Omega_S}\left[n_1e_{15}\phi_{,1}^i(\mathbf{x})+n_2e_{15}\phi_{,2}^i(\mathbf{x})+n_3e_{33}\phi_{,3}^i(\mathbf{x})\right]d\Gamma\right)=0 \tag{24}$$

$$\sum_{i=1}^{n}\hat{u}_1^i\left(\int_{\partial\Omega_S}\left[n_1e_{15}\phi_{,3}^i(\mathbf{x})+n_3e_{31}\phi_{,1}^i(\mathbf{x})\right]d\Gamma\right)+\sum_{i=1}^{n}\hat{u}_2^i\left(\int_{\partial\Omega_S}\left[n_2e_{15}\phi_{,3}^i(\mathbf{x})+n_3e_{31}\phi_{,2}^i(\mathbf{x})\right]d\Gamma\right)$$
$$+\sum_{i=1}^{n}\hat{u}_3^i\left(\int_{\partial\Omega_S}\left[n_1e_{15}\phi_{,1}^i(\mathbf{x})+n_2e_{15}\phi_{,2}^i(\mathbf{x})+n_3e_{33}\phi_{,3}^i(\mathbf{x})\right]d\Gamma\right) \tag{25}$$
$$-\sum_{i=1}^{n}\hat{\psi}^i\left(\int_{\partial\Omega_S}\left[n_1h_{11}\phi_{,1}^i(\mathbf{x})+n_2h_{11}\phi_{,2}^i(\mathbf{x})+n_3h_{33}\phi_{,3}^i(\mathbf{x})\right]d\Gamma\right)-\sum_{i=1}^{n}\hat{M}^i\left(\int_{\Omega_S}q\phi^i(\mathbf{x})d\Omega\right)=0$$

$$\sum_{i=1}^{n}\hat{\psi}^i\left(qM_0\int_{\partial\Omega_S}\left[n_1\mu_{11}\phi_{,1}^i(\mathbf{x})+n_2\mu_{22}\phi_{,2}^i(\mathbf{x})+n_3\mu_{33}\phi_{,3}^i(\mathbf{x})\right]d\Gamma\right)$$
$$+\sum_{i=1}^{n}\hat{M}^i\left(q\int_{\partial\Omega_S}\left[n_1d_{11}\phi_{,1}^i(\mathbf{x})+n_2d_{22}\phi_{,2}^i(\mathbf{x})+n_3d_{33}\phi_{,3}^i(\mathbf{x})\right]d\Gamma\right)=0 \tag{26}$$

Equations (22-26) are considered on the sub-domains adjacent to interior nodes as well as to the boundary nodes on Γ_{st}, Γ_{sq} and Γ_{sb}. Complete system of partial differential equations for the computation of the nodal unknowns can be obtained by collecting the discretized local boundary-domain integral equations together with the discretized boundary conditions. Collocation approach is used to impose essential boundary conditions directly, using MLS variable approximations (19). For natural boundary conditions local integral equations are written for the nodes on the appropriate segments of the global boundary as explained in [12].

4. Numerical examples

Results of numerical experiments are presented in this section to show applicability of the proposed MLPG formulation for the analysis of piezoelectric semiconducting cylindrical

body. Variety of piezoelectric devices (sensors) have cylindrical shape. A three dimensional cylinder with radius $R = 0.015\text{m}$ and height $h = 0.001\text{m}$ is considered. Homogeneous material properties are selected to test the present computational method. The material coefficients of the cylinder are considered for aluminum nitride (AlN) according to [8]:

$$c_{11} = c_{22} = 40.3 \cdot 10^{10}\, Nm^{-2}\ , \qquad c_{12} = 14.3 \cdot 10^{10}\, Nm^{-2}\ , \qquad c_{13} = c_{23} = 10.4 \cdot 10^{10}\, Nm^{-2}\ ,$$
$$c_{33} = 38.2 \cdot 10^{10}\, Nm^{-2}\ , \quad c_{44} = c_{55} = 3.53 \cdot 10^{10}\, Nm^{-2}\ ,$$
$$e_{15} = -0.39\, Cm^{-2}\ , \quad e_{31} = -0.66\, Cm^{-2}\ , \quad e_{33} = 1.57\, Cm^{-2}\ ,$$
$$h_{11} = h_{22} = h_{33} = 0.8092 \cdot 10^{-10} C(Vm)^{-1}\ , \quad \mu_{11} = \mu_{22} = \mu_{33} = 3.0 \cdot 10^{-2} m^2 (Vs)^{-1}\ ,$$
$$d_{11} = d_{22} = d_{33} = 7.0 \cdot 10^{-4} m^2 s^{-1}\ , \quad q = 1.602 \cdot 10^{-19}\, C$$

The geometry of the cylinder is discretized with using 1204 nodal points as shown on Fig. 2. The radius of the MLS support domain is chosen as $r^i = 0.007\text{m}$. The bottom of the assumed cylinder is clamped corresponding to state when it is placed on a rigid support, thus all components of mechanical displacements are set to zero. Vanishing electric potential and the change of electron density are prescribed at the bottom side that corresponds to the grounding electrode attached there. Vertical displacements, induced electric potential and the change of electron density are measured at the top of the cylinder. Three initial electron densities M_0 are considered in numerical examples corresponding to conducting ($M_0 = 1e^6, 1e^7$ [m^{-3}]) and non-conducting/dielectric ($M_0 = 0.0$ [m^{-3}]) cases.

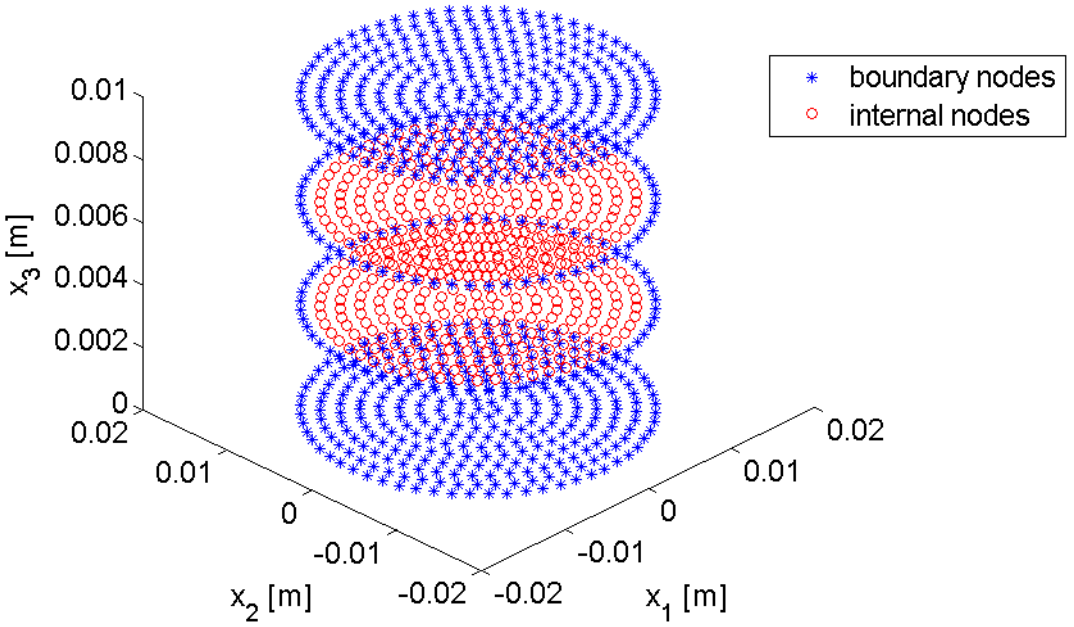

Fig. 2. Distribution of 1204 nodal points over the considered cylinder.

In the first numerical example a uniform electric potential load $\psi(x_1, x_2, x_3 = h) = 100V$ is defined at the top of the cylinder. As noted in [22] a uniform load will cause axially symmetric response and thus axisymmetric analysis can also be performed. Obtained results are compared to FEM-Comsol solution that is using 3900 elements. Variation of vertical displacement u_3 along the line on the top of the cylinder (x_1; $x_2 = 0$; $x_3 = h$) is depicted on Fig. 3. One can see that the initial electron density M_0 has almost vanishing influence on the

resulting vertical displacement. Variation of electron density M with x_1 coordinate is shown on Fig. 4. Initial electron densities have in this case significant influence on the resulting electron density M. For the vanishing initial electron density (dielectric piezoelectric material) we obtain also vanishing resulting electron density.

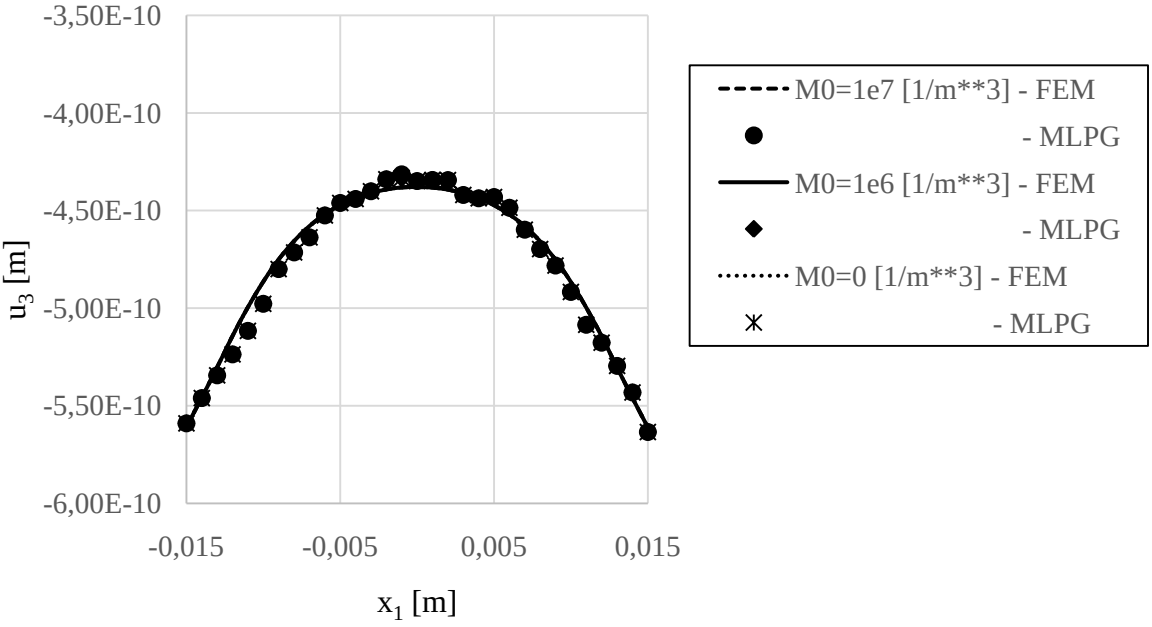

Fig. 3. Variation of vertical displacement u_3 with x_1 coordinate for the case of conducting and non-conducting piezoelectric material under electric potential load.

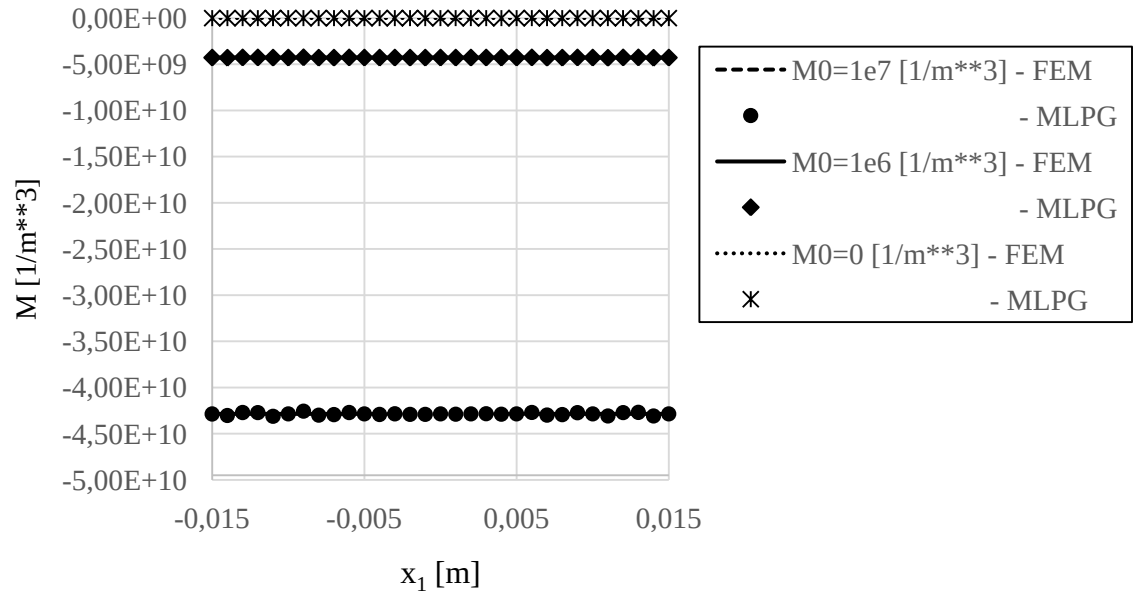

Fig. 4. Variation of change of electron density M with x_1 coordinate for the case of conducting and non-conducting piezoelectric material under electric potential load.

In the second numerical example a non-uniform mechanical traction load is prescribed at the top of the cylinder. In general engineering applications the applied load have non-uniform distribution. Then 3D numerical analysis is required. In the case considered here, the distribution of the vertical traction field over the nodal points on the top side of the cylindrical cylinder is governed by formula

$$T_3^{top}\left(x_1, x_2, x_3 = h\right) = a \cdot \sin\left(\pi \frac{x_1 + b}{R}\right) \tag{27}$$

where a, b are arbitrary constants. For the compressive load considered here the constants are taken as $a = 1.0 \times 10^4$ and $b = 0.01$. Fig. 5 shows the schematic variation of the prescribed traction in x_1 direction over the top side of cylinder.

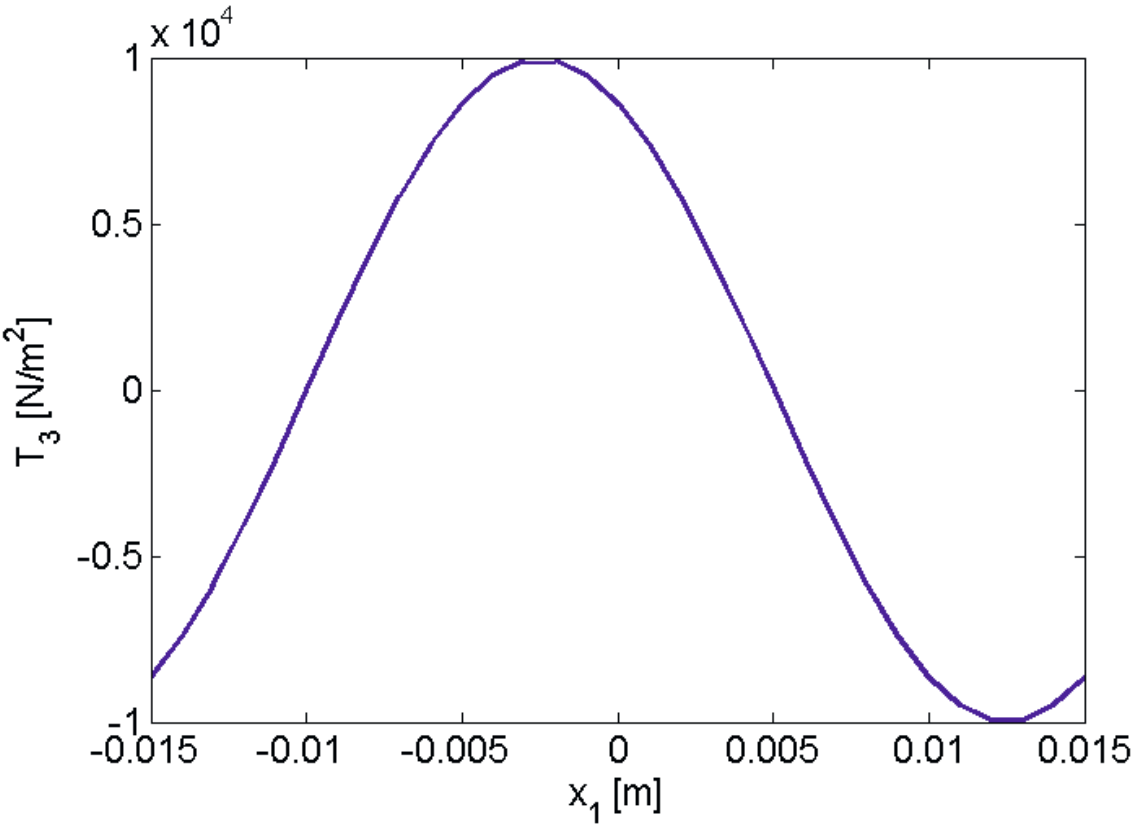

Fig. 5. Variation of the prescribed traction field over the cylinder.

Obtained results are again compared to FEM-Comsol solution that is using 3900 elements. Variation of vertical displacement u_3 along the line on the top of the cylinder ($x_1;\ x_2 = 0;\ x_3 = h$) is depicted on Fig.6. The response of induced electric potential to the applied non-uniform compressive load is shown in Fig. 7 and induced electron density in Fig. 8. Excellent agreement between FEM and MLPG results is observed.

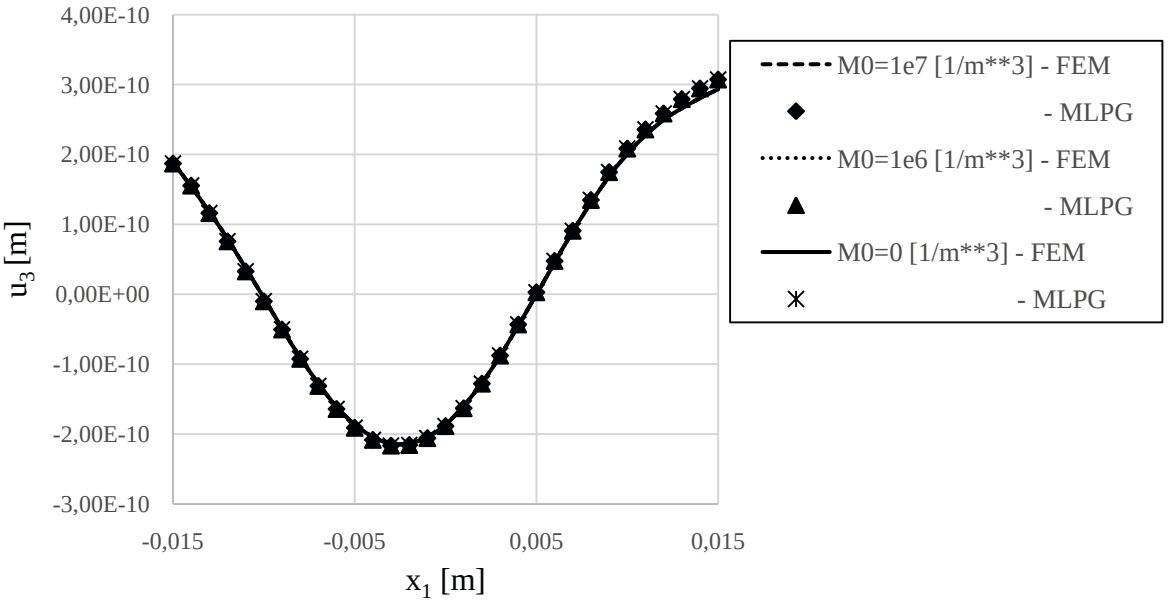

Fig. 6. Variation of vertical displacement u_3 with x_1 coordinate for the case of conducting and non-conducting piezoelectric material.

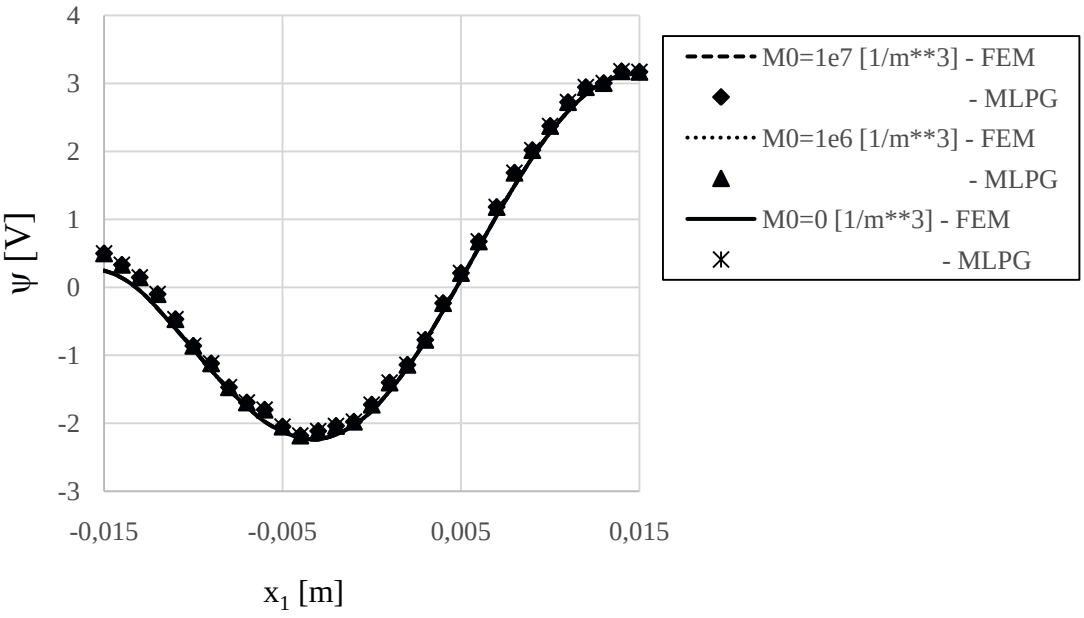

Fig. 7. Variation of electric potential ψ with x_1 coordinate for the case of conducting and non-conducting piezoelectric material.

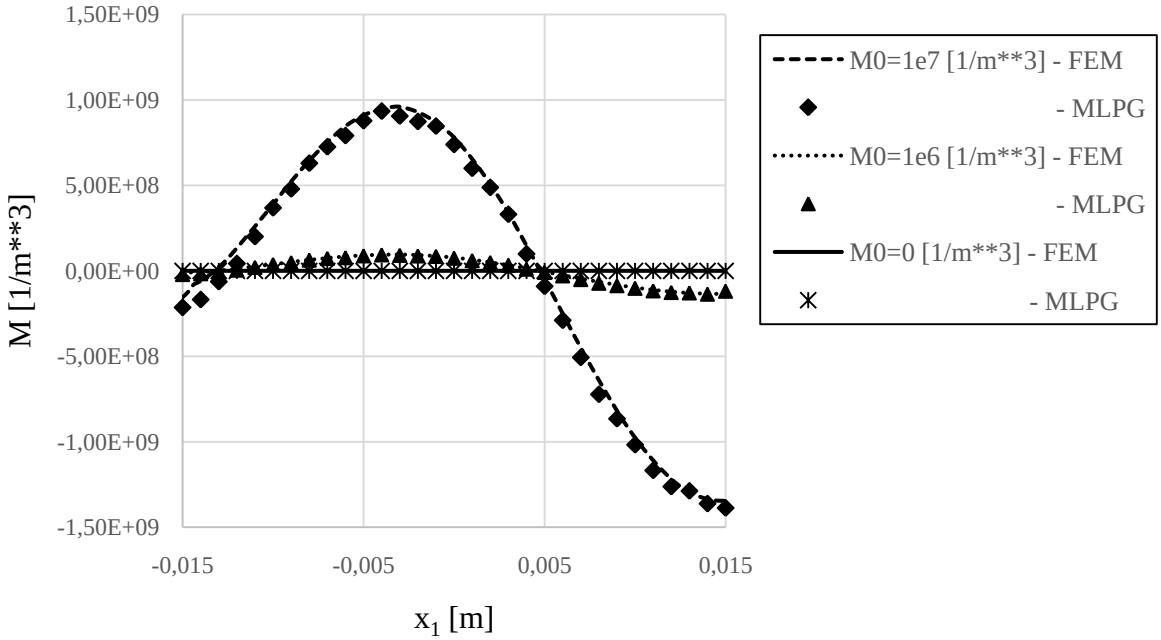

Fig. 8. Variation of change of electron density M with x_1 coordinate for the case of conducting and non-conducting piezoelectric material.

One can observe from Figs. 6 and 7 that the influence of the density of electrons in unloaded state M_0 on the mechanical displacement and electric potential responses to considered loadings is negligible. However, the variation of the change of electron density $M(\mathbf{x})$ along the x_1 coordinate is strongly influenced by the initial electron density M_0 as can be seen on Fig. 8. This can be explained as follows. The r.h.s. in the governing equation (2) and the boundary condition $n_i D_i(\mathbf{x}) = qM(\mathbf{x})$ can be approximately neglected, since the electric charge of the electron is very small as compared with other material coefficients. Furthermore, the constitutive laws (4) and (5) are independent on the density of electrons in unloaded state M_0 as well as on the change of electron density $M(\mathbf{x})$. Then, the boundary value problem for the primary fields $u_i(\mathbf{x})$ and $\psi(\mathbf{x})$ can be solved separately from the b.v.p. for the change of electron density $M(\mathbf{x})$.

Overall responses of the electric potential and the free electron density at the top of the cylinder are shown on Fig. 9 for the conducting piezoelectric case with $M_0 = 10^6\ m^{-3}$.

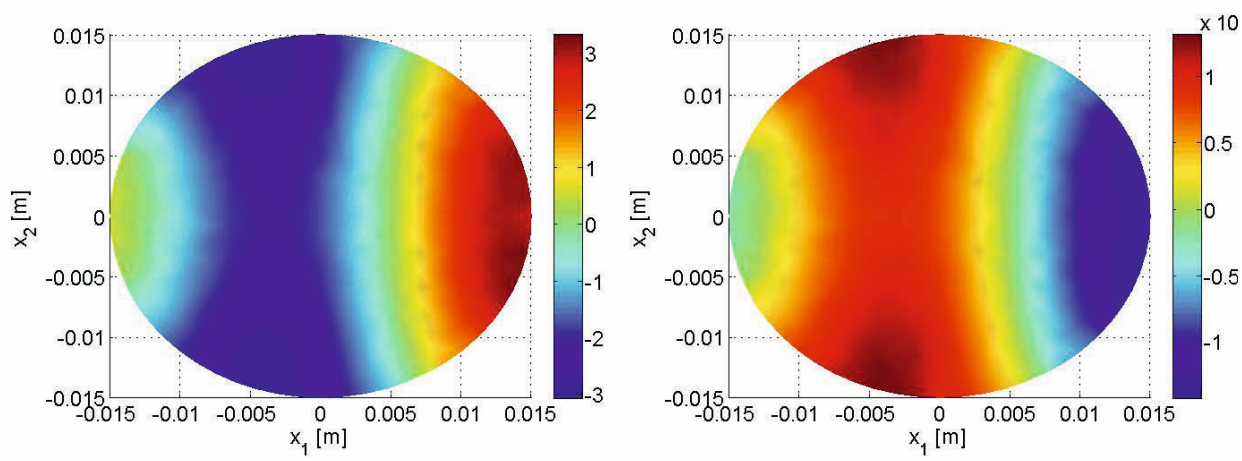

a) b)

Fig. 9.Field variations at the top of the piezoelectric semiconducting cylinder under mechanical load: a) electric potential; b) electron density.

Finally, combined mechanical and electron density load is considered to assess the influence of conducting piezoelectric properties on the response of the cylinder thus enabling us to observe interactions occurring in acoustoelectric effect. Mechanical traction load is has the same variation and value as in the previous example (see Eq. 27). Non-zero value of the free electron density $M(x_1, x_2, x_3 = h) = 10^{15} m^{-3}$ is prescribed on the top side of the cylinder. Initial electron density is kept as $M_0 = 10^7 m^{-3}$. Since electron density is prescribed as a boundary condition, initial electron density will have no influence on its value. Fig. 10 shows variation of vertical displacement u_3 with x_1 coordinate while on Fig. 11 the variation of induced electric potential ψ with x_1 coordinate is shown for the case of the pure mechanical load and the combined mechanical and free electron density load.

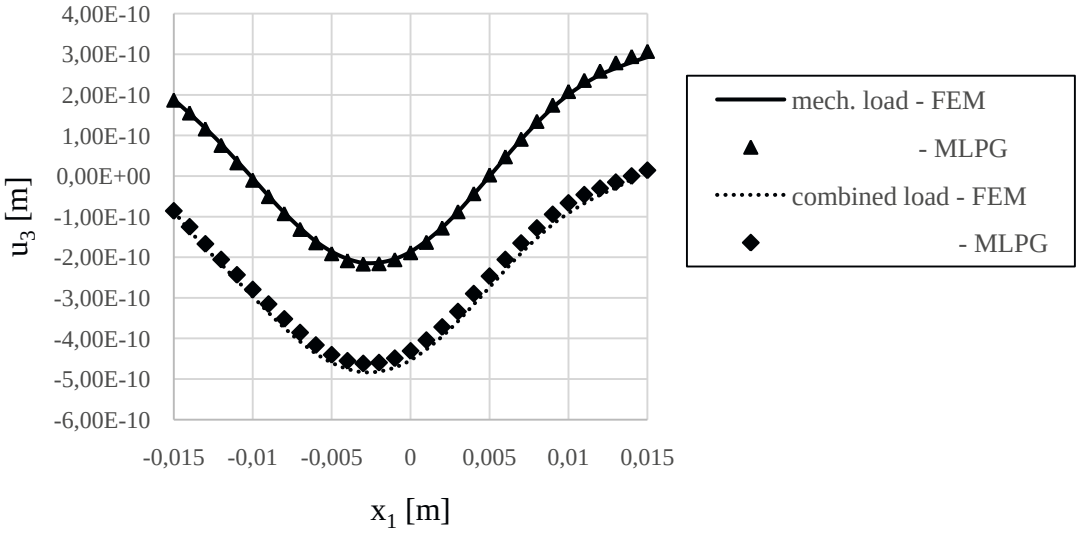

Fig. 10. Variation of vertical displacement u_3 with x_1 coordinate for the case of pure mechanical and combined load.

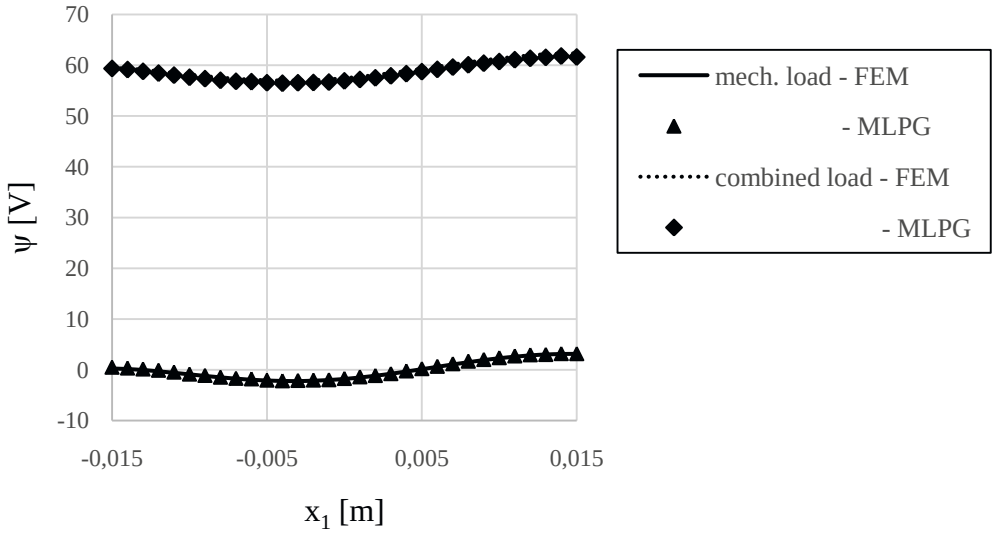

Fig. 11. Variation of electric potential ψ with x_1 coordinate for the case of pure mechanical and combined load.

Significant change of both vertical displacements and induced electric potentials can be observed on Figs. 10 and 11 if nonzero electron densities are prescribed indicating vast possibilities in control of mechanical and electrical response of piezoelectric structures if piezoelectric semiconductors are used instead of piezoelectric dielectric materials.

Excellent agreement between FEM and MLPG results is again observed indicating that MLPG is a promising method for the analysis of piezoelectric semiconductors using much lower number of nodal points compared to FEM.

Conclusion

A meshless local Petrov-Galerkin method (MLPG) is proposed in this paper for the solution of boundary value problems for coupled electro-mechanical fields in 3D piezoelectric semiconductors. Proposed method is a truly meshless method as no discretization elements were used for the approximation or integration of unknowns. The MLS approximation scheme has been used for approximation of trial functions. Using the Heaviside unit step function as a test function pure boundary formulation on each local subdomain has been obtained.

The main advantage of the present method is its simplicity and generality in comparison to other techniques such as the conventional BEM. The method is particularly promising for problems which cannot be solved by the conventional BEM in cases when the fundamental solutions are not available.

Applicability of proposed meshless method is demonstrated on numerical example assuming non-uniform loading and conducing and non-conducting conditions. Results indicate that initial electron density has negligible influence on resulting mechanical displacement and electric potential responses under mechanical load. However significant difference has been observed in responses when a pure mechanical load was applied and when the mechanical load was combined with essential boundary conditions for the free electron density. Presented meshless method may be easily extended also to design of functionally graded piezoelectric semiconducting devices in the future.

Acknowledgement

The authors gratefully acknowledge the support by the Slovak Science and Technology Assistance Agency registered under number APVV-14-0216.

REFERENCES:

[1] SONG, G.-SETHI, V.-Li, H.N.: Engineering Structures, *28*, 2006, p.1513.

[2] TIERSTEN, H. F.: Linear Piezoelectric Plate Vibrations, Plenum, New York, 1969.

[3] TIERSTEN, H. F.-SHAM, T. L.: IEEE Transactions on Ultrasonics, Ferroelectrics and Frequency Control, *45*, 1998, p. 1.

[4] DU, J.-JIN, X.-WANG, J.: In: 2007 IEEE International Frequency Control Symposium Joint with the 21st European Frequency and Time Forum. IEEE 2007. p. 749.

[5] WHITE, D. L.: Journal of Applied Physics, *33*, 1962, p. 2547.

[6] GHOSH, S. K.: Indian Journal of Pure and Applied Physics, *44*, 2006, p.183.

[7] BUYUKKOSE, S.-HERNANDEZ-MINGUEZ, A.- VRATZOV, B.- et al.: Nanotechnology, 25, 2014, p.135204.

[8] SLADEK, J.-SLADEK, V.-PAN, E.-WUNSCHE, M.: Engineering Fracture Mechanics, 126, 2014, p.27.

[9] BENJEDDOU, A.: Computers and Structures, 76, 2000, p. 347.

[10] LEE, J.S.: Engineering Analysis with Boundary Elements, 15, 1995, p. 321.

[11] DING, H.-LIANG, J.: Computers & Structures, 71, 1999, p. 447.

[12] ATLURI, S. N.: The Meshless Method (MLPG) For Domain & BIE Discretizations. Forsyth: Tech Science Press, 2004.

[13] SLADEK, J.-SLADEK, V.-ATLURI, S.N.: CMES: Computer Modeling in Engineering & Sciences, 6, 2004, p. 477.

[14] SLADEK, J.-SLADEK, V.-ZHANG, Ch.-GARCIA-SANCHEZ, F.-WUNSCHE, M.: CMC: Computers, Materials & Continua, 4, 2006, p. 109.

[15] SLADEK, J.-SLADEK, V.-ZHANG, Ch.-SOLEK, P.-STAREK, L.: CMES: Computer Modeling in Engineering & Sciences, 19, 2007, p. 247.

[16] SLADEK, J.-SLADEK, V.-STANAK, P.: Acta Mechanica Slovaca, 14, 2010, p. 16.

[17] SLADEK, J.-SLADEK, V.-STANAK, P.-PAN, E.: CMES – Computer Modeling in Engineering and Sciences, 64, 2010, p. 267.

[18] SLADEK, J.-SLADEK, V.-STANAK, P.-WEN, P. H.-ATLURI, S. N.: CMES – Computer Modeling in Engineering and Sciences, 85, 2012, p. 543.

[19] SLADEK, J.-SLADEK, V.-STANAK, P.-ZHANG, Ch.-WUNSCHE, M.: Engineering Structures, 47, 2013, p. 81.

[20] STANAK, P.-SLADEK, J.-SLADEK, V.-KRAHULEC, S.: Building Research Journal, 59, 2011, pp. 125.

[21] SLADEK, J.-SLADEK, V.-SOLEK, P.: CMES: Computer Modeling in Engineering & Sciences, 43, 2009, p. 223.

[22] STANAK, P.-TADEU, A.-SLADEK, J.-SLADEK,V.: Journal of Intelligent Material Systems and Structures, 2014, DOI: 10.1177/1045389X14549864 (In Press)

[23] DONG, L.- ALOTAIBI, A.- MOHIUDDINE, S.A.-ATLURI, S. N.:. CMES: Computer Modeling in Engineering and Sciences, *99*, 2014, p.1.

[24] LANCASTER, P.-SALKAUSKAS, T.: Mathematics in Computation, 37, 1981, p. 141.